Freeze-Thaw Stress: Effects of Temperature on Hydraulic Conductivity and Ultrasonic Activity in Ten Woody Angiosperms[1]

Guillaume Charrier[2]*, Katline Charra-Vaskou[2], Jun Kasuga, Hervé Cochard, Stefan Mayr, and Thierry Améglio

Department of Botany, University of Innsbruck, A–6020 Innsbruck, Austria (G.C., S.M.); and Institut National de la Recherche Agronomique, Clermont Université, and Université Blaise Pascal, Unité Mixte de Recherche 547, Physique et Physiologie Intégratives de l'Arbre Fruitier et Forestier, F–63100 Clermont-Ferrand, France (K.C.-V., J.K., H.C., T.A.)

Freeze-thaw events can affect plant hydraulics by inducing embolism. This study analyzed the effect of temperature during the freezing process on hydraulic conductivity and ultrasonic emissions (UE). Stems of 10 angiosperms were dehydrated to a water potential at 12% percentage loss of hydraulic conductivity (PLC) and exposed to freeze-thaw cycles. The minimal temperature of the frost cycle correlated positively with induced PLC, whereby species with wider conduits (hydraulic diameter) showed higher freeze-thaw-induced PLC. Ultrasonic activity started with the onset of freezing and increased with decreasing subzero temperatures, whereas no UE were recorded during thawing. The temperature at which 50% of UE were reached varied between −9.1°C and −31.0°C across species. These findings indicate that temperatures during freezing are of relevance for bubble formation and air seeding. We suggest that species-specific cavitation thresholds are reached during freezing due to the temperature-dependent decrease of water potential in the ice, while bubble expansion and the resulting PLC occur during thawing. UE analysis can be used to monitor the cavitation process and estimate freeze-thaw-induced PLC.

Xylem embolism is a limiting factor for plant survival and distribution (Choat et al., 2012; Charrier et al., 2013). Two major factors can induce embolism in the xylem of plants: drought and freeze stress. Freeze-thaw-induced embolism is caused by bubbles formed during freezing that then expand on thawing (Lemoine et al., 1999; Hacke and Sperry, 2001; Cruiziat et al., 2002; Tyree and Zimmermann, 2002). As wider conduits contain more gas and form larger bubbles, which expand at less negative tension, conduit diameter and xylem sap tension are critical for the formation of freeze-thaw-induced embolism (Davis et al., 1999; Pittermann and Sperry, 2003). Accordingly, Mayr and Sperry (2010) observed a loss of conductivity only when samples were under critical tension during thawing. Under drought stress, tension in the xylem sap increases the sensitivity to embolism generated by successive freeze-thaw cycles (Mayr et al., 2003, 2007).

Ultrasonic emissions (UE) analysis can be used to detect cavitation events in wood. It is unclear how well related UE are to cavitation events, as they are extracted from continuous acoustic emissions and depend on set definitions. However, UE analysis has been proven effective for monitoring drought-induced embolism in the laboratory (Pena and Grace, 1986; Salleo and Lo Gullo, 1986; Borghetti et al., 1993; Salleo et al., 2000) as well as in field experiments (Ikeda and Ohtsu, 1992; Jackson et al., 1995; Jackson and Grace, 1996; Hölttä et al., 2005; Ogaya and Penuelas, 2007). In a cavitating conduit, signals are probably produced by the disruption of the water column and subsequent tension relaxation of cell walls.

UE have also been detected during freezing events, but the origin of these signals was less clear. In some cases, UE were observed during thawing, which are thus probably related to embolism formation according to the classic thaw-expansion hypothesis (Mayr and Sperry, 2010); however, all species studied have produced UE on freezing, which cannot yet be explained (Raschi et al., 1989; Kikuta and Richter, 2003; Mayr et al., 2007; Mayr and Sperry, 2010; Mayr and Zublasing, 2010). The low solubility of gases in ice prompted the idea that air bubbles expulsed from the ice structure produce UE near the ice-liquid interface (Sevanto et al., 2012). As the water potential of ice is strongly temperature dependent, the minimum temperature during freezing might be a relevant factor. Numerous studies have analyzed UE patterns during freeze-thaw cycles in conifers

[1] This work was supported by the Agence Nationale de la Recherche and Fonds zur Förderung der Wissenschaftlichen Forschung (grant no. I826–B25, "Acoufreeze").

[2] These authors contributed equally to the article.

* Address correspondence to guillaume.charrier@uibk.ac.at.

The author responsible for distribution of materials integral to the findings presented in this article in accordance with the policy described in the Instructions for Authors (www.plantphysiol.org) is: Guillaume Charrier (guillaume.charrier@uibk.ac.at).

www.plantphysiol.org/cgi/doi/10.1104/pp.113.228403

(Mayr et al., 2007; Mayr and Sperry, 2010; Mayr and Zublasing, 2010) or angiosperms (Weiser and Wallner, 1988; Kikuta and Richter, 2003), but few of them measured embolism concomitantly. Percentage loss of hydraulic conductivity (PLC) was only measured in a few studies and only in conifers (Mayr et al., 2007; Mayr and Sperry, 2010).

In this study, we analyzed the effect of freeze-thaw cycles on the hydraulic conductivity and ultrasonic activity in 10 angiosperm species. We hypothesized that (1) the extent of freeze-thaw-induced embolism depends on xylem anatomy (related to conduit diameter) and minimal temperature (related to the water potential of ice); (2) ultrasonic activity is also influenced by anatomy and temperature; and (3) PLC and UE are positively correlated. PLC was measured in 10 angiosperm species after freeze-thaw cycles at different minimal temperatures (−10 to −40°C). Furthermore, UE were recorded during a freeze-thaw cycle down to −40°C.

RESULTS

PLC increased significantly after one freeze-thaw cycle in all species (Fig. 1). Conductivity was also influenced by minimal temperature in most species. PLC increased significantly with decreasing minimal temperature in *Coryllus avelana*, *Juglans regia*, *Prunus cerasus*, *Prunus persica*, *Salix alba*, and *Sorbus aucuparia*, increased only slightly in *Crataegus monogyna* and *Fagus sylvatica*, and increased not at all in *Betula pendula* and *Prunus cerasifera*. Across all species, significant correlations were observed between the minimal temperature and freeze-thaw-induced PLC (r^2 = 0.307, $P < 0.001$; Fig. 2A). This increase in PLC is also significantly correlated to mean hydraulically weighted vessel diameter (D_h; Fig. 2B) for minimal temperature of −20°C ($P < 0.001$), −30°C ($P = 0.034$), and −40°C ($P = 0.009$) but not −10°C ($P = 0.329$). Statistically, minimal temperature (θ) and D_h were both significantly correlated to PLC ($P < 0.001$), but their interaction was significantly stronger than their single effect in predicting freeze-thaw-induced PLC ($\theta \times D_h$, $P = 0.036$; θ, $P = 0.97$; D_h, $P = 0.67$ with $r^2 = 0.672$).

In *J. regia*, UE were generated between the onset of freezing in the wood (dotted line in Fig. 3A) and when minimum temperature was reached. No UE were recorded during the temperature plateau at −40°C or during thawing. Across replicates, the total number of UE after one freeze-thaw cycle was variable (i.e. from 50,000 to 1,000,000 in *J. regia*), but relative cumulated ultrasonic emissions (cumUE) during a freeze-thaw cycle showed little variability (Fig. 3A). The plot of cumUE versus temperature revealed a sigmoidal curve (r^2 = 0.989, $P < 0.001$), with an increase in ultrasonic activity until approximately −17°C and a decrease at lower temperatures (Fig. 3B). In November, there was a shift in the relationship between cumUE and temperature in *J. regia*. The temperature generating 50% of cumulated ultrasonic emissions (T_{50}) decreased from −16.8°C to −21.5°C, and the curve slope decreased.

Minimal temperatures had a differential effect on UE generation across species (Fig. 4). In *J. regia*, UE were generated during four successive cycles with decreasing minimal temperatures, with half of all UE recorded during the −30°C cycle. In *F. sylvatica*, most UE were also generated during the −30°C cycle (82% of total UE), whereas in *Sorbus aucuparia*, most UE were generated during the −40°C cycle (90% of total UE). In all species, UE were only recorded when temperatures fell below those reached in previous cycles (Fig. 4).

All species produced a similar sigmoid pattern of cumUE versus temperature ($r^2 > 0.928$ and $r^2 > 0.975$ in nine species), but temperature thresholds differed across species: temperatures inducing 50% of cumUE ranged from −9.2°C in *B. pendula* to −31.0°C in *Sorbus aucuparia* (Table I). Across species, cumUE at −10°C,

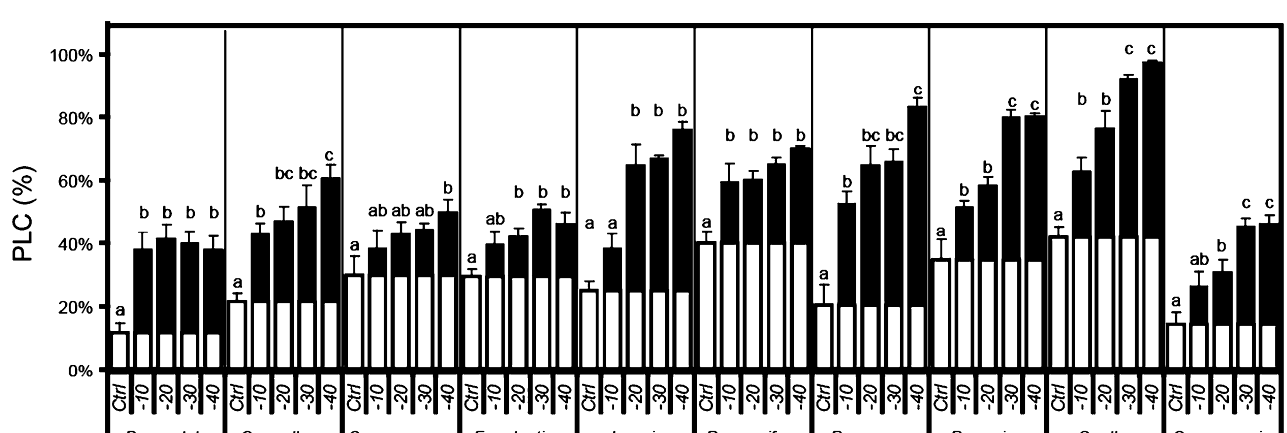

Figure 1. PLC after dehydration to a water potential at 12% PLC (control) and exposure to one freeze-thaw cycle down to different minimal temperatures (−10°C, −20°C, −30°C, or −40°C). Black parts of columns indicate differences in PLC from the control. Different letters represent significantly different losses of conductivity within each species.

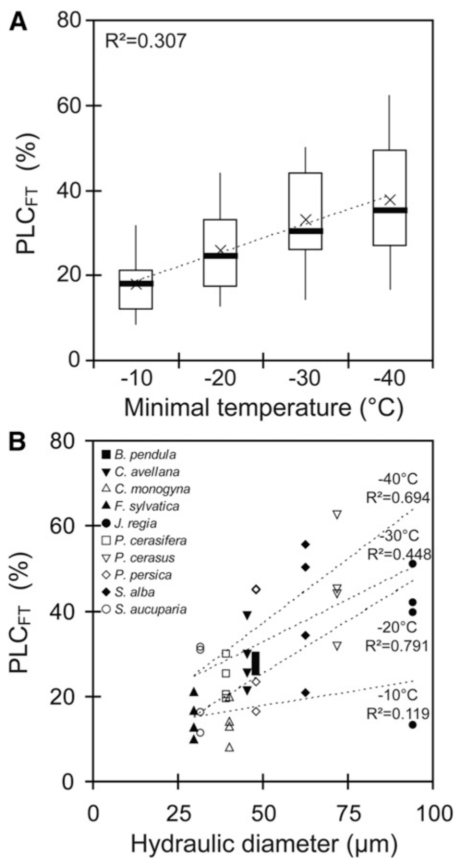

Figure 2. A, Increase in PLC induced by a freeze-thaw cycle (PLC_{FT}) versus minimal temperature in 10 angiosperm species (first and ninth deciles, extreme lines; first and third quartiles, extremities of the rectangle; median, black lines; mean, crosses). B, Increase in PLC generated by a freeze-thaw cycle depending on mean hydraulic diameter of vessels in 10 angiosperm species.

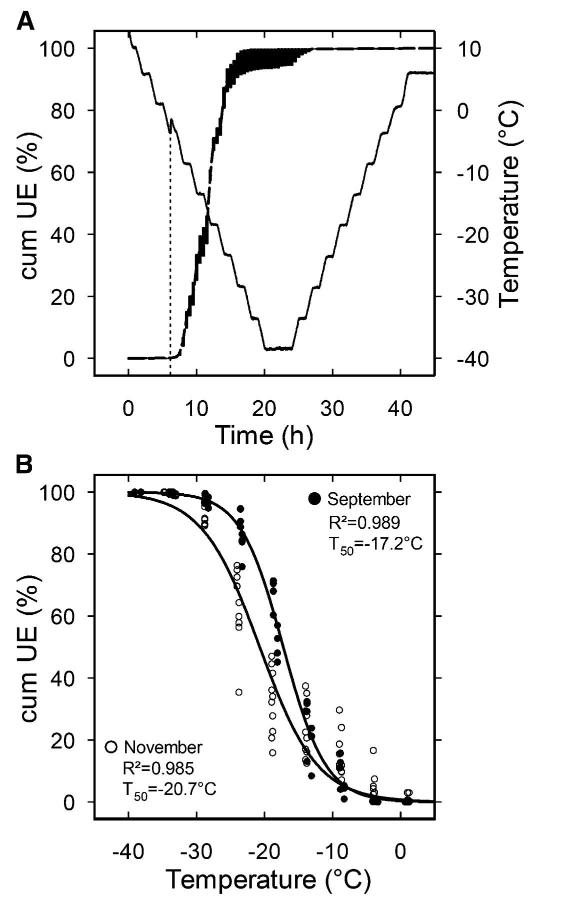

Figure 3. A, Dynamic of cumUE (means ± SE; n = 4 replicates; dashed line) during a freeze-thaw cycle (black line) in *J. regia*. The dotted line charts the appearance of an exotherm. B, Relative cumUE depending on temperature from the same experiment in September (black circles) and November (white circles fitted). Black lines represent the sigmoid fit of the data.

−20°C, and −30°C were significantly correlated to the relative PLC (r^2 = 0.653, P < 0.001; Fig. 5).

Across species, T_{50} was significantly correlated to water potential inducing 50% PLC (r^2 = 0.517, P = 0.010; Fig. 6). In drought-sensitive species (Table II), T_{50} was less negative (e.g. −9.2°C in *B. pendula* and −14.6°C in *Salix alba*) than in drought-resistant species (e.g. −31.0°C in *Sorbus aucuparia* and −24.6°C in *P. cerasifera*).

DISCUSSION

In the studied angiosperm species, freeze-thaw-induced PLC increased with decreasing minimal temperature (Figs. 1 and 2A), as also demonstrated by Pockman and Sperry (1997) and Ball et al. (2006) on angiosperms, but in contrast to Mayr and Sperry (2010) on a conifer. Freeze-thaw-induced PLC was also positively correlated with D_h. A similar relationship was previously described in laboratory experiments on conifers (Davis et al., 1999; Pittermann and Sperry, 2003, 2006) and angiosperms (Stuart et al., 2007; Choat et al., 2011) and in field studies (Charrier et al., 2013; Schreiber et al., 2013).

Temperatures also influenced ultrasonic activity during the freezing process, as cumUE increased with falling temperatures (Fig. 3). As in conifers (Mayr et al., 2007; Mayr and Zublasing, 2010) and other angiosperms

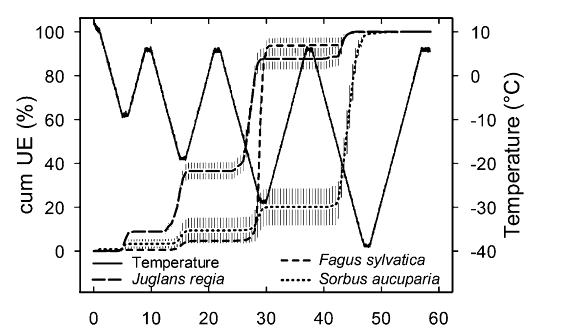

Figure 4. The cumUE in partially dehydrated *J. regia* (long dashed line), *F. sylvatica* (short dashed line), and *Sorbus aucuparia* (dotted line) after freeze-thaw cycles at successively lower minimal temperatures (−10°C, −20°C, −30°C, and −40°C; black line). A value of 100% represents cumUE after four freeze-thaw cycles for each species.

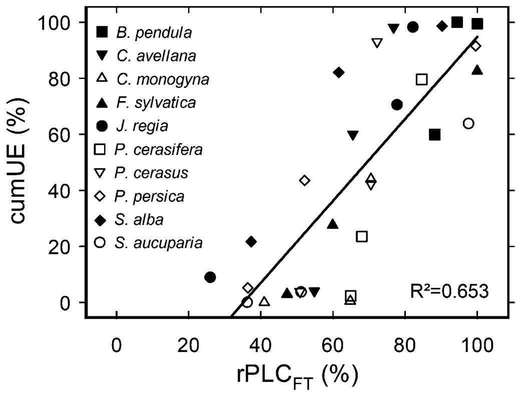

Figure 5. Relation between cumUE generated at −10°C, −20°C, or −30°C during a freeze-thaw cycle down to −40°C and relative PLC generated after a freeze-thaw cycle ($rPLC_{FT}$) down to −10°C, −20°C, or −30°C.

(Weiser and Wallner, 1988; Raschi et al., 1989; Lo Gullo and Salleo, 1993), UE were never detected before freezing temperatures were reached. The cumUE versus temperature curves followed a sigmoid pattern in *J. regia* (Fig. 3B) and other species (Table I). These curves were highly variable across species, with temperatures inducing 50% of cumUE ranging from −9.2°C (*B. pendula*) to −31°C (*Sorbus aucuparia*). In *J. regia*, we observed a seasonal shift in the temperature dependence of ultrasonic activity (Fig. 3B). In November, the trees that had suffered two moderate natural freezing events could have been weakened (e.g. "frost fatigue" in Christensen-Dalsgaard and Tyree, 2013), but this would have resulted in a translated curve (similar slope and higher T_{50}). Here, the curve showed a gentler slope and lower T_{50}, which may indicate cold acclimation (Dowgert and Steponkus, 1983). Hydraulic acclimation has not previously been observed (Charra-Vaskou et al., 2012). We suggest that a fraction of UE were derived from living cells and able to acclimate. Protoplast fragmentation and ultrastructural changes in xylem ray parenchyma cells have been cited as a potential source of UE during freezing (Weiser and Wallner, 1988; Ristic and Ashworth, 1993). The ratio of signals from living cells to signals from conduits is unclear, but the process could explain why angiosperm wood, which contains more living cells, generated far more UE (hundreds of thousands) than conifer wood (several hundreds). Planned studies of the intrinsic parameters of acoustic signals (e.g. amplitude and energy) may bring insights into the sources of UE, as done for drought stress, from xylem (approximately 25%) and symplast cavitation (approximately 75% in Wolkerstorfer et al., 2012).

Freeze-thaw-induced PLC and UE were positively correlated, as both were dependent on temperature during the freezing process (Fig. 5). Another probable source of UE during freezing is the formation of bubbles in xylem conduits, while the formation of embolism and the resulting PLC occurs during thawing (Mayr and Sperry, 2010). According to Sevanto et al. (2012), two mechanisms are likely involved in air bubble formation during freezing: gas segregation and air seeding from a previously air-filled conduit. The solubility of air is 1,000 times lower in ice than in liquid water (Morris and McGrath, 1981). Gases ejected from the ice structure concentrate at the ice-liquid interface and nucleate in

Table I. *r^2 and parameters (T_{50} and slope) calculated from ultrasonic activity versus temperature curves fitted with sigmoid function*

Boldface indicates drought-sensitive species.

Species	r^2	T_{50}	Slope
		°C	*% °C^{-1}*
B. pendula	0.981	−9.2	−0.48
Coryllus avelana	0.985	−18.9	−0.36
Crataegus monogyna	0.984	−30.5	−0.50
F. sylvatica	0.928	−23.8	−0.25
J. regia	0.989	−17.2	−0.32
P. cerasifera	0.991	−24.6	−0.25
P. cerasus	0.978	−21.1	−0.29
P. persica	0.994	−21.0	−0.26
Salix alba	0.993	−14.6	−0.28
Sorbus aucuparia	0.975	−31.0	−0.42

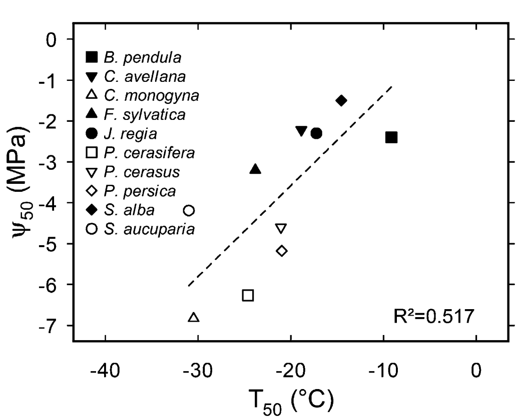

Figure 6. Relation between water potential generating 50% loss of conductivity (Ψ_{50}) and T_{50}.

Table II. *Water potentials inducing 50% (Ψ_{50}) and 12% (Ψ_{12}) loss of conductivity (from Choat et al., 2012)*

Boldface indicates drought-sensitive species.

Species	Ψ_{50}	Ψ_{12}
	MPa	
B. pendula	−2.40	−1.50
Coryllus avelana	−2.22	−1.97
Crataegus monogyna	−6.83	−5.40
F. sylvatica	−3.20	−2.00
J. regia	−2.30	−1.87
P. cerasifera	−6.27	−5.60
P. cerasus	−4.60	−4.02
P. persica	−5.18	−3.81
Salix alba	−1.50	−1.00
Sorbus aucuparia	−4.19	−2.20

a bubble, releasing tension in conduits and probably emitting UE (Davitt et al., 2010). Many more UE are detected during freezing than during drying, especially in species with wider conduits (Kikuta and Richter, 2003). Anatomic studies did not detect bubbles in frozen conduits using the cryo-scanning electron microscopy technique (Utsumi et al., 1998; Ball et al., 2006; Cobb et al., 2007), but this technique potentially induces artifacts (Cochard et al., 2000), as rapid freezing velocities (i.e. faster than 75 μm s^{-1} as induced by liquid nitrogen) entrap the gas into ice without forming bubbles (Sperry and Robson, 2001) or induce bubble sizes that fall below the resolution of the microscope system (Sevanto et al., 2012). Nevertheless, at a slower freezing rate, bubbles of approximately 2 μm in diameter were observed in the center of lumens (Robson et al., 1988).

The water potential at the ice-liquid interface decreases with decreasing temperature as the potential of ice changes at a ratio of approximately -1 MPa K^{-1} (Hansen and Beck, 1988; Cavender-Bares, 2005). Another factor to consider is that solutes (e.g. salts and carbohydrates) have a lower solubility in ice than in liquid water and are thus concentrated in the remaining liquid volumes near the ice-liquid interface (Sevanto et al., 2012). The enormous effect of temperature on the water potential may cause bubbles to expand or air seeding from adjacent, already air-filled conduits (Sperry and Tyree 1990; Cochard et al., 1992). Samples already at critical tension (e.g. water potential generating 12% loss of conductivity, as in the samples used here) are probably most affected and thus generate many UE (Mayr and Zublasing, 2010). Air seeding is the underlying mechanism of drought-induced embolism (Hacke and Sperry, 2001), which may explain the observed link between the temperature dependence of UE activity and the vulnerability to drought-induced embolism (Fig. 6). This correlation indicates that air seeding plays a role in drought-induced as well as freeze-thaw-induced embolism. Pit membrane porosity is a crucial factor for air seeding (Lens et al., 2011), and future studies should focus on possible links between pit structures and vulnerability to freezing-induced embolism. Furthermore, the temperature of ice nucleation in the sap is lower and the cavitation threshold is higher in species with small conduits than in species with wider conduits, which also tends to link both mechanisms (Lintunen et al., 2013). It is also possible that minimal temperature may not affect PLC in some species (*B. pendula*, *P. cerasifera* [Fig. 1], and *P. contorta* [Mayr and Sperry, 2010]) because of their xylem anatomy. Small plasmodesmatal pores in pits could prevent air seeding (Jansen et al., 2009), and scalariform plates could stop air passing through perforations (Tyree and Zimmermann, 2002). Both minimal temperature and anatomy thus play important roles in freeze-thaw-induced PLC (Fig. 2).

Bubbles and air-water menisci in pits are blocked by the arriving ice front and can only expand at thawing (Cruiziat et al., 2002), depending on the water potential in the surrounding sap and the bubble radius (Ewers, 1985; Davis et al., 1999; Pittermann and Sperry, 2003). Wider conduits contain more dissolved gases and, consequently, more bubbles after freezing. At thawing, coalesced bubbles may more easily reach the critical radius (Sperry and Sullivan, 1992; Davis et al., 1999; Pittermann and Sperry, 2003). The proposed mechanism is schematized in Figure 7.

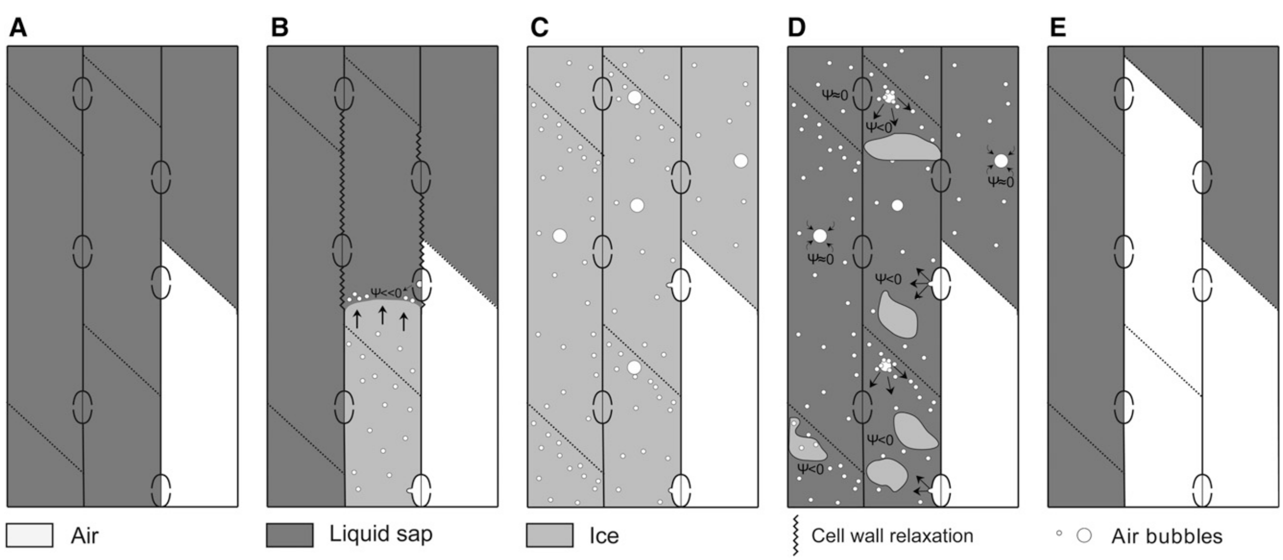

Figure 7. Proposed mechanism of freeze-thaw-induced embolism. In moderately dehydrated samples, some vessels are air filled (white) before freezing (A). During freezing, ice (light gray) propagates through vessels (arrows), air nucleates near the ice-water interface, and a local, low water potential ($\Psi << 0$) induces air seeding from air-filled vessels. This leads to relaxation of the tension in cell walls and the emission of ultrasonic waves (B). Bubbles of different size (white circles) are entrapped by the arriving ice front (C) but can coalesce and dilate during thawing when the tension is low enough ($\Psi < 0$; D), thus inducing embolism (E).

CONCLUSION

Subzero temperatures play an important role in the formation of freeze-thaw-induced embolism and ultrasonic activity during freezing. Damage to living cells may be a source of UE. However, the temperature-dependent decrease in water potential likely influences bubble formation and air seeding in xylem conduits during the freezing process, with the thresholds for these processes being dependent on anatomical structures. UE can be used to monitor the cavitation process during freezing and to estimate the resulting loss of conductivity detected after complete freeze-thaw cycles.

MATERIALS AND METHODS

Plants

Ten European tree species were chosen that differed in anatomy and resistance to drought-induced embolism (Table II). Branches, 1 m in length, were harvested during the growing season (from July to September) from trees at natural sites in Austria (Innsbruck) or France (Clermont-Ferrand). In addition, *Juglans regia* was also harvested after leaf fall (end of November). Samples were wrapped in plastic bags, and the base was kept in water. The basal diameter of twigs was around 2 cm. On the laboratory bench, branches were dehydrated to a water potential generating 12% loss of conductivity (±0.2 MPa; Table I). Water potential was measured on end twigs using a Scholander pressure chamber (model 1000 pressure chamber; PMS Instrument). Samples were cut to 50 cm, and side branches were removed. Samples were then tightly wrapped in Parafilm (Alcan) to prevent further dehydration.

Freeze-Thaw Treatments

Samples were exposed to freeze-thaw treatments in a temperature-controlled chamber (MK999 [Clermont-Ferrand] or MK53 [Innsbruck]; Binder). The following experiments were performed. (1) All species were exposed to one freeze-thaw cycle down to −40°C with thawing to +5°C. Temperature changed at 5 K h^{-1} but remained constant at every 5 K step (on freezing and thawing). Air temperature was held constant for 4 h at minimal temperature before thawing. (2) *Fagus sylvatica*, *J. regia*, and *Sorbus aucuparia* were exposed to four successive freeze-thaw cycles to −10°C, −20°C, −30°C, and −40°C with thawing to +5°C between cycles. Temperature changed at 5 K h^{-1} and was held constant for 1 h at minimal and maximal temperatures.

Detection of UE

UE acquisition was performed on an eight-channel SAMOS (Euro-Physical Acoustics) or a PCI-8 system (Physical Acoustics) equipped with 150-kHz resonance sensors (R15; 80–400 kHz) connected to a preamplifier set to 40 decibels. Approximately 1 cm^2 of the bark was removed from the underside of samples (opposite side of tension wood) using a razor blade, and the debarked surface was covered with silicone grease to prevent further transpiration and optimize acoustic coupling. The sensors were tightly clamped to the debarked parts of the samples. The acoustic detection threshold was set to 45 decibels. UE recording and analysis were performed using AEwin software (Mistras Holdings). The cumUE was calculated as a percentage of total UE recorded during an experiment. Air temperature in the temperature-controlled chamber and xylem temperatures of sample twigs were measured using copper-constantan thermocouples connected to a datalogger (CR3000 [Clermont-Ferrand] or CR10X [Innsbruck]; Campbell Scientific).

Hydraulic Conductivity Measurements

Hydraulic conductivity was measured on independent samples harvested and prepared in the same way as for acoustic measurements. Samples were exposed to different minimal temperatures (−10°C, −20°C, −30°C, and −40°C) with temperature courses similar to experiment 1 above. Control branches were kept at 5°C overnight. PLC was measured with a Xyl'Em embolism meter (Cochard et al., 2000). Samples, 7 cm in length, were submerged in water and cut with a scalpel to prevent air entry into vessels (n = 5–10 per species and temperature). Initial conductance (k_i) was measured using a solution of KCl (0.01 mol L^{-1}) and $CaCl_2$ (0.001 mol L^{-1}) at low pressure (3.50 kPa). After perfusing the same solution at high pressure (140 kPa) to remove embolism, conductance was remeasured. Measurements and flushing were repeated twice until maximal conductance (k_{max}) was reached. PLC was then calculated as:

$$PLC = (k_{max} - k_i)/k_{max} \quad (1)$$

For correlations analysis, different hydraulic parameters were calculated.

$$PLC_{FT} = PLC - PLC_{control} \quad (2)$$

where PLC_{FT} is the freeze-thaw-induced PLC and $PLC_{control}$ is the PLC without the freeze-thaw cycle.

$$rPLC = \frac{PLC - PLC_{control}}{PLC_{max} - PLC_{control}} \quad (3)$$

where rPLC is the relative PLC and PLC_{max} is the maximal PLC measured after one freeze-thaw cycle among all tested temperatures.

Anatomy

Samples were progressively included in polyethylene glycol (Carbowax; Dow) and then cut into 19-μm-thick slices using a cryomicrotome (Reichert). Cells were lysed using sodium hypochlorite (5 g L^{-1}) for 15 to 30 min. Samples were rinsed with acetic acid (1% [v/v]) and stained with safranin (1% [v/v]) for 3 to 5 min. Stained tissues were successively washed with water and 50% (v/v), 70% (v/v), and 100% (v/v) ethanol. Cross sections were then observed with a microscope (400×), and images were analyzed using ImageJ software (1.45s; National Institutes of Health). Three different 1- × 1-mm images were analyzed per species. Diameters of vessels were measured using the analyze particles function, and mean D_h was calculated using the Hagen-Poiseuille equation, which states that water flow in a capillary is proportional to the fourth power of the radius:

$$D_h = \sqrt[4]{\frac{\Sigma d^4}{n}} \quad (4)$$

where d is the individual vessel diameter.

Statistical Analysis

After testing for Gaussian distribution, we calculated linear regression and P values using R software (R Development Core Team, 2005). Multiple linear regression was calculated by r^2 minimization using the lm function in the R software.

ACKNOWLEDGMENTS

We thank Christian Bodet and Pierre Conchon for their help with the hydraulic conductivity and anatomy measurements and two anonymous reviewers for their valuable comments on the first version of the manuscript.

Received September 13, 2013; accepted December 15, 2013; published December 16, 2013.

LITERATURE CITED

Ball MC, Canny MJ, Huang CX, Egerton JJG, Wolfe J (2006) Freeze/thaw-induced embolism depends on nadir temperature: the heterogeneous hydration hypothesis. Plant Cell Environ **29:** 729–745

Borghetti M, Grace J, Raschi AE, editors (1993) Water Transport in Plants under Climatic Stress. Cambridge University Press, Cambridge, UK

Cavender-Bares J (2005) Impacts of freezing on long-distance transport in woody plants. *In* NM Holbrook, MA Zwieniecki, eds, Vascular Transport in Plants. Elsevier Academic Press, Amsterdam, pp 401–424

Charra-Vaskou K, Charrier G, Wortemann R, Beikircher B, Cochard H, Améglio T, Mayr S (2012) Drought and frost resistance of trees: a

comparison of four species at different sites and altitudes. Ann For Sci **69:** 325–333
Charrier G, Cochard H, Améglio T (2013) Evaluation of the impact of frost resistances on potential altitudinal limit of trees. Tree Physiol **33:** 891–902
Choat B, Jansen S, Brodribb TJ, Cochard H, Delzon S, Bhaskar R, Bucci SJ, Feild TS, Gleason SM, Hacke UG, et al (2012) Global convergence in the vulnerability of forests to drought. Nature **491:** 752–755
Choat B, Medek DE, Stuart SA, Pasquet-Kok J, Egerton JJG, Salari H, Sack L, Ball MC (2011) Xylem traits mediate a trade-off between resistance to freeze-thaw-induced embolism and photosynthetic capacity in overwintering evergreens. New Phytol **191:** 996–1005
Christensen-Dalsgaard KK, Tyree MT (2013) Does freezing and dynamic flexing of frozen branches impact the cavitation resistance of *Malus domestica* and the *Populus* clone Walker? Oecologia **173:** 665–674
Cobb AR, Choat B, Holbrook NM (2007) Dynamics of freeze-thaw embolism in Smilax rotundifolia (Smilacaceae). Am J Bot **94:** 640–649
Cochard H, Bodet C, Améglio T, Cruiziat P (2000) Cryo-scanning electron microscopy observations of vessel content during transpiration in walnut petioles: facts or artifacts? Plant Physiol **124:** 1191–1202
Cochard H, Cruiziat P, Tyree MT (1992) Use of positive pressures to establish vulnerability curves: further support for the air-seeding hypothesis and implications for pressure-volume analysis. Plant Physiology **100:** 205–209
Cruiziat P, Cochard H, Améglio T (2002) Hydraulic architecture of trees: main concepts and results. Ann For Sci **59:** 723–752
Davis SD, Sperry JS, Hacke UG (1999) The relationship between xylem conduit diameter and cavitation caused by freezing. Am J Bot **86:** 1367–1372
Davitt K, Arvengas A, Caupin F (2010) Water at the cavitation limit: density of the metastable liquid and size of the critical bubble. Europhys Lett **90:** 16002
Dowgert MF, Steponkus PL (1983) Effect of cold acclimation on intracellular ice formation in isolated protoplasts. Plant Physiol **72:** 978–988
Ewers FW (1985) Xylem structure and water conduction in conifer trees, dicot trees, and lianas. IAWA Bull **6:** 309–317
Hacke UG, Sperry JS (2001) Functional and ecological xylem anatomy. Perspect Plant Ecol Evol Syst **4:** 97–115
Hansen J, Beck E (1988) Evidence for ideal and non-ideal equilibrium freezing of leaf water in frost hardy ivy (*Hedera helix*) and winter barley (*Hordeum vulgare*). Bot Acta **101:** 76–82
Hölttä T, Vesala T, Nikinmaa E, Perämäki M, Siivola E, Mencuccini M (2005) Field measurements of ultrasonic acoustic emissions and stem diameter variations: new insight into the relationship between xylem tensions and embolism. Tree Physiol **25:** 237–243
Ikeda T, Ohtsu M (1992) Detection of xylem cavitation in field-grown pine trees using the acoustic emission technique. Ecol Res **7:** 391–395
Jackson GE, Grace J (1996) Field measurements of xylem cavitation: are acoustic emissions useful? J Exp Bot **47:** 1643–1650
Jackson GE, Irvine J, Grace J (1995) Xylem cavitation in two mature Scots pine forests growing in a wet and a dry area of Britain. Plant Cell Environ **18:** 1411–1418
Jansen S, Choat B, Pletsers A (2009) Morphological variation of intervessel pit membranes and implications to xylem function in angiosperms. Am J Bot **96:** 409–419
Kikuta SB, Richter H (2003) Ultrasound acoustic emissions from freezing xylem. Plant Cell Environ **26:** 383–388
Lemoine D, Granier A, Cochard H (1999) Mechanism of freeze-induced embolism in *Fagus sylvatica* L. Trees **13:** 206–210
Lens F, Sperry JS, Christman MA, Choat B, Rabaey D, Jansen S (2011) Testing hypotheses that link wood anatomy to cavitation resistance and hydraulic conductivity in the genus *Acer*. New Phytol **190:** 709–723
Lintunen A, Hölttä T, Kulmala M (2013) Anatomical regulation of ice nucleation and cavitation helps trees to survive freezing and drought stress. Sci Rep **3:** 2031
Lo Gullo MA, Salleo S (1993) Different vulnerabilities of *Quercus ilex* L. to freeze- and summer drought-induced xylem embolism: an ecological interpretation. Plant Cell Environ **16:** 511–519
Mayr S, Cochard H, Améglio T, Kikuta SB (2007) Embolism formation during freezing in the wood of *Picea abies*. Plant Physiol **143:** 60–67
Mayr S, Gruber A, Bauer H (2003) Repeated freeze-thaw cycles induce embolism in drought stressed conifers (Norway spruce, stone pine). Planta **217:** 436–441
Mayr S, Sperry JS (2010) Freeze-thaw-induced embolism in *Pinus contorta*: centrifuge experiments validate the 'thaw-expansion hypothesis' but conflict with ultrasonic emission data. New Phytol **185:** 1016–1024
Mayr S, Zublasing V (2010) Ultrasonic emissions from conifer xylem exposed to repeated freezing. J Plant Physiol **167:** 34–40
Morris GJ, McGrath JJ (1981) Intracellular ice nucleation and gas bubble formation in *Spirogyra*. Cryo Lett **2:** 341–352
Ogaya R, Penuelas J (2007) Seasonal ultrasonic acoustic emissions of *Quercus ilex* L. trees in a Mediterranean forest. Acta Physiol Plant **29:** 407–410
Pena J, Grace J (1986) Water relations and ultrasound emissions of *Pinus sylvestris* L. before, during and after a period of water stress. New Phytol **103:** 515–524
Pittermann J, Sperry JS (2003) Tracheid diameter is the key trait determining the extent of freezing-induced embolism in conifers. Tree Physiol **23:** 907–914
Pittermann J, Sperry JS (2006) Analysis of freeze-thaw embolism in conifers: the interaction between cavitation pressure and tracheid size. Plant Physiol **140:** 374–382
Pockman WT, Sperry JS (1997) Freezing-induced xylem cavitation and the northern limit of *Larrea tridentata*. Oecologia **109:** 19–27
R Development Core Team (2005) R: A Language and Environment for Statistical Computing. R Foundation for Statistical Computing, Vienna
Raschi A, Scarascia Mugnozza G, Surace R, Valentini R, Vazzana C (1989) The use of ultrasound technique to monitor freezing and thawing of water in plants. Agric Ecosyst Environ **27:** 411–418
Ristic Z, Ashworth EN (1993) Ultrastructural evidence that intracellular ice formation and possibly cavitation are the sources of freezing injury in supercooling wood tissue of *Cornus florida* L. Plant Physiol **103:** 753–761
Robson DJ, McHardy WJ, Petty JA (1988) Freezing in conifer xylem. 2. Pit aspiration and bubble formation. J Exp Bot **39:** 1617–1621
Salleo S, Lo Gullo MA (1986) Xylem cavitation in nodes and internodes of whole *Chorisia insignis* H. B. et K. plants subjected to water stress: relations between xylem conduit size and cavitation. Ann Bot (Lond) **58:** 431–441
Salleo S, Nardini A, Pitt F, Lo Gullo MA (2000) Xylem cavitation and hydraulic control of stomatal conductance in laurel (*Laurus nobilis* L.). Plant Cell Environ **23:** 71–79
Schreiber SG, Hamann A, Hacke UG, Thomas BR (2013) Sixteen years of winter stress: an assessment of cold hardiness, growth performance and survival of hybrid poplar clones at a boreal planting site. Plant Cell Environ **36:** 419–428
Sevanto S, Holbrook NM, Ball MC (2012) Freeze/thaw-induced embolism: probability of critical bubble formation depends on speed of ice formation. Front Plant Sci **3:** 107
Sperry JS, Robson DG (2001) Xylem cavitation and freezing in conifers. *In* S Colombo, F Bigras, eds, Conifer Cold Hardiness. Kluwer Academic Publishers, Dordrecht, The Netherlands, pp 121–136
Sperry JS, Sullivan JE (1992) Xylem embolism in response to freeze-thaw cycles and water stress in ring-porous, diffuse-porous, and conifer species. Plant Physiol **100:** 605–613
Sperry JS, Tyree MT (1990) Water-stress-induced xylem embolism in three species of conifers. Plant Cell Environ **13:** 427–436
Stuart SA, Choat B, Martin KC, Holbrook NM, Ball MC (2007) The role of freezing in setting the latitudinal limits of mangrove forests. New Phytol **173:** 576–583
Tyree MT, Zimmermann MH (2002) Xylem Structure and the Ascent of Sap. Springer-Verlag, Berlin
Utsumi Y, Sano Y, Fujikawa S, Funada R, Ohtani J (1998) Visualization of cavitated vessels in winter and refilled vessels in spring in diffuse-porous trees by cryo-scanning electron microscopy. Plant Physiol **117:** 1463–1471
Weiser RL, Wallner SJ (1988) Freezing woody plant stems produces acoustic emissions. J Am Soc Hortic Sci **113:** 636–639
Wolkerstorfer SV, Rosner S, Hietz P (2012) An improved method and data analysis for ultrasound acoustic emissions and xylem vulnerability in conifer wood. Physiol Plant **146:** 184–191